Journal of Power Sources 196 (2011) 8735–8741

Contents lists available at ScienceDirect

Journal of Power Sources

journal homepage: www.elsevier.com/locate/jpowsour

# Multi-parameter battery state estimator based on the adaptive and direct solution of the governing differential equations

Shuoqin Wang[a,*], Mark Verbrugge[b], John S. Wang[a], Ping Liu[a]

[a] HRL Laboratories, LLC, Malibu, CA, United States
[b] Chemical Sciences and Materials Systems Lab, General Motors R&D, Warren, MI, United States

ARTICLE INFO

*Article history:*
Received 20 May 2011
Received in revised form 22 June 2011
Accepted 22 June 2011
Available online 29 June 2011

*Keywords:*
Battery state estimator
BSE algorithm
SOC (state of charge) estimation
SOP (state of power) estimation
Equivalent circuit model

ABSTRACT

We report the development of an adaptive, multi-parameter battery state estimator based on the direct solution of the differential equations that govern an equivalent circuit representation of the battery. The core of the estimator includes two sets of inter-related equations corresponding to discharge and charge events respectively. Simulation results indicate that the estimator gives accurate prediction and numerically stable performance in the regression of model parameters. The estimator is implemented in a vehicle-simulated environment to predict the state of charge (SOC) and the charge and discharge power capabilities (state of power, SOP) of a lithium ion battery. Predictions for the SOC and SOP agree well with experimental measurements, demonstrating the estimator's application in battery management systems. In particular, this new approach appears to be very stable for high-frequency data streams.

© 2011 Elsevier B.V. All rights reserved.

## 1. Introduction

Lithium ion batteries have attracted great interest for automotive applications due to their high energy and power density, wide temperature range, and long cycle life [1–7]. In order to realize the full benefit of these traction batteries, efficient energy management is essential. In many battery-powered systems such as electric vehicles (EV) and hybrid electric vehicles (HEV), energy efficiency is enhanced by intelligent management of the electrochemical energy storage system [8]. These applications require a battery state estimator (BSE) to ensure accurate and timely estimation of the state of charge (SOC), the charge and the discharge power capabilities (SOP), and the state of health (SOH).

Various battery models have been studied within the framework of a BSE [9–24]. A physics based electrochemical model may be able to capture the temporally evolved and spatially distributed behavior of the essential states of a battery [9,10,23]. It is built upon fundamental laws of transport, kinetics and thermodynamics, and requires inputs of many physical parameters [24]. Because of its complexity, relative long-simulation time, and difficult control of the output, this kind of model may be more suitable for battery design and analysis rather than a BSE. A (zero dimensional) lumped parameter approach based on an equivalent circuit model may be more suitable for a practical BSE due to ease of implementation. The single RC circuit model discussed in this paper is a simple and apparently robust approach that has been studied for the aforementioned purposes of a BSE [14,21,22,25,26]. It should be noted that this approach is fundamentally correct only when the battery is exposed to small signal perturbations around equilibrium. Highly non-equilibrium behavior of the battery is difficult to address. For such behavior, more physical effects need to be included along with a more detailed model, at the expense of the simplicity and robustness [11–13,20].

Many state estimators employ a superposition integration (SI) scheme [25,27–30] to predict in real-time the SOC, SOP, and SOH. This approach has been applied to Li-ion (lithium ion), lead acid, and NiMH batteries wherein the SI algorithm is based on a simple one-RC-circuit model of the battery as shown in Fig. 1. Inputs to the algorithm include the battery current, voltage, and temperature; the algorithm is used to regress the model parameters such as the open circuit voltage ($V_{oc}$), the high-frequency resistance ($R$), the charge-transfer resistance ($R_{ct}$) and capacitance ($C$). SOC, SOP and SOH can then be determined using the model parameters. Due to limited memory storage and computing speed of embedded controllers employed in many applications, the algorithm has been implemented with recursive relations using circuit parameters from previous time steps and experimental measurements acquired in the current-time step to regress new circuit parameters. The method of weighted recursive least squares (WRLS) is employed in the SI algorithm, wherein input

* Corresponding author. Tel.: +1 310 317 5183; fax: +1 310 317 5840.
*E-mail address:* swang@hrl.com (S. Wang).

0378-7753/$ – see front matter © 2011 Elsevier B.V. All rights reserved.
doi:10.1016/j.jpowsour.2011.06.078

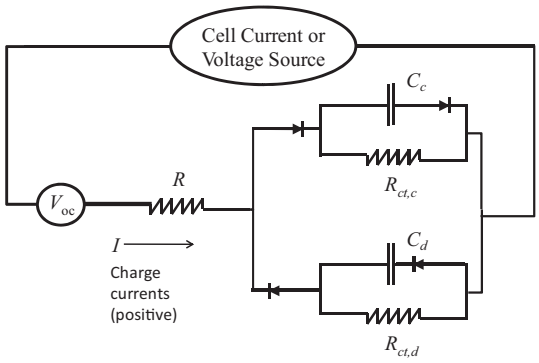


**Fig. 1.** Equivalent circuit employed in this work for the battery. Positive current corresponds to charging.

data is damped exponentially over time. As a result, newer information has a preferential impact on the value of regressed parameters.

We have found that the aforementioned SI algorithm becomes unstable at high sampling rates (e.g., for date-sampling frequencies above 10 Hz). As part of this work, the SI algorithm was applied to amorphous carbon/NMC (nickel, manganese, cobalt oxide) batteries (Hitachi cells intended for GM's high-voltage Belt/Alternator/Starter application, termed BAS+) and tested in a simulated HEV environment [31]. We also found that the numerical stability of the regression of the model parameters was sensitive to initial (seed) values. This sensitivity often led to numerical anomalies in the parameter regression. Both of above mentioned instabilities might be due to the fact that the SI algorithm is intrinsically a nonlinear model. Inside the model a "measured" term is the function of the parameter to be determined [25]. In addition, the current SI algorithm uses only one set of model parameters to describe both the charge and discharge events for the battery. In order to accommodate the possibility of different electrode kinetics processes for charge and discharge [32,33], the SI algorithm employed a fixed parameter $r = R_{ct,\,\mathrm{charge}}/R_{ct,\,\mathrm{discharge}}$, which represented the ratio between the values of $R_{ct}$ for cell charge relative to discharge. Similarly, the charge-transfer time-constant, which is the multiplication of the $R_{ct}$ and $C$, was assumed to be the same for both events.

In order to address these shortcomings, we have developed an improved battery state estimator, which we refer to as the direct differential (DD) algorithm. Similar to the SI algorithm, the DD algorithm employs the one RC-circuit model shown in Fig. 1 and the WRLS method to regress model parameters in real-time. Hence, the DD algorithm outputs the SOC, SOP, and SOH (deduced from changes in the regressed impedance parameters relative to those of a new, healthy battery) with the inputs of the voltage, current and temperature. Unlike SI, the DD algorithm is a strict linear model. Consequently, we have observed much more stable parameter regression upon application to simulated data. The algorithm treats the charge and discharge events separately; therefore there is no need for the fixed parameter $r$. Overall, implementation of the DD algorithm showed superior performance compared with the SI algorithm, including less sensitivity to initial (seed) parameter values and better stability at high sampling rates.

This report is organized as follows. Section 2 details the derivation of the DD algorithm; Section 3 overviews the algorithm's regression capability through the use of simulated data; Section 4 describes the experimental setup including essential hardware and software elements; and experimental results are presented and discussed in Section 5. These include parameter regression in real-time, SOC prediction via Coulomb titration results, and 2 s and 10 s power projections. Finally, summary and open questions are provided in Section 6.

## 2. The direct differential algorithm

The application of Kirchhoff's circuit laws using the one RC-circuit model in Fig. 1 produces the following differential equation:

$$V = (R + R_{ct})I + RR_{ct}C\frac{dI}{dt} - R_{ct}C\frac{dV}{dt} + V_{oc} \tag{1}$$

All of the symbols in the equation are defined in Fig. 1; $V$ and $I$ are measured inputs (their time derivatives being derived directly from measurements) and $R$, $R_{ct}$, $C$, and $V_{oc}$ are model parameters regressed at each time step. Therefore, the formalism corresponds to a parameter identification problem in the control theory [34]. Positive currents correspond to charge (cf. Fig. 1). In order to address the differences between the charge and discharge kinetic processes, Eq. (1) is expanded into the following:

$$\begin{aligned} V = {} & \left[(R + R_{ct})I + RR_{ct}C\frac{dI}{dt} - R_{ct}C\frac{dV}{dt} + V_{oc}\right]_c \\ & + \left[(R + R_{ct})I + RR_{ct}C\frac{dI}{dt} - R_{ct}C\frac{dV}{dt} + V_{oc}\right]_d \\ = {} & (R_c + R_{ct\_c})I_c + R_cR_{ct\_c}C_c\left(\frac{dI}{dt}\right)_c - R_{ct\_c}C_c\left(\frac{dV}{dt}\right)_c + V_{oc\_c} \\ & + (R_d + R_{ct\_d})I_d + R_dR_{ct\_d}C_d\left(\frac{dI}{dt}\right)_d - R_{ct\_d}C_d\left(\frac{dV}{dt}\right)_d + V_{oc\_d} \end{aligned} \tag{2}$$

In this equation, all model parameters and variables with the subscript "$d$" are associated with the discharge process, while those with the subscript "$c$" are with the charge process. Unlike the aforementioned SI algorithm, the DD algorithm explicitly treats the discharge and charge cases separately. The parameters are regressed by applying the measured values of the current $I$ and voltage $V$ of the battery in real-time. The derivatives of the current and voltage over time are approximated with the difference equations; i.e., $dI/dt = (I(t) - I(t - \Delta t))/\Delta t$ and $dV/dt = (V(t) - V(t - \Delta t))/\Delta t$. (A central difference formulation can be employed to achieve higher numerical accuracy.) If the current $I$ is positive (charging), $I_c = I$, $(dI/dt)_c = dI/dt$, $(dV/dt)_c = dV/dt$, and all variables associated with discharge are set to zero. The same convention holds for discharge currents. In the application to the Li-ion batteries of this work, we simplify Eq. (2) by assuming $R_d = R_c = R$ since the observed difference between the high-frequency-impedance for charging and discharging events is small. Fig. 2 depicts the cell potential of the Li-ion battery as a function of SOC. Since there is only slight hysteresis at the C/3 rate, it is reasonable to assume that the hysteresis is minimal for the $V_{oc}$ vs. SOC relationship; hence, $V_{oc\_c} = V_{oc\_d} = V_{oc}$. The final equation of the DD algorithm for the Li-Ion battery estimator becomes:

$$\begin{aligned} V = {} & (R + R_{ct\_c})I_c + RR_{ct\_c}C_c\left(\frac{dI}{dt}\right)_c - R_{ct\_c}C_c\left(\frac{dV}{dt}\right)_c \\ & + (R + R_{ct\_d})I_d + RR_{ct\_d}C_d\left(\frac{dI}{dt}\right)_d - R_{ct\_d}C_d\left(\frac{dV}{dt}\right)_d + V_{oc} \end{aligned} \tag{3}$$

The WRLS method is applied to regress the model parameters. The method is briefly described as follows. Consider a linear dynamical model with input variables $\{x_l(t),\ l = 1, 2, \ldots, L\}$ and output variable $y(t)$ and assume these variables are sampled at discrete

times $\{t_j, j = 1, 2, 3, \ldots, N\}$ and further assume that the sampled values can be related through the linear equation

$$y(t_j) = \sum_{l=1}^{L} m_l x_l(t_j) \tag{4}$$

where $\{m_l, l = 1, 2, \ldots, L\}$ are the $L$ parameters to be identified. In the WRLS method, the parameters are determined by minimizing the sum of the weighted square of the error terms: [25]

$$\varepsilon = \sum_{l=1}^{L} \varepsilon_l = \sum_{l=1}^{L} \sum_{j=1}^{N} \lambda_l^{N-j} \left[ y(t_j) - \sum_{l=1}^{L} m_l x_l(t_j) \right]^2, \tag{5}$$

where $\{\lambda_l, l = 1, 2...L\}$ are the $L$ exponential forgetting factors for time-weighting data. A larger weight factor $\lambda_l$ gives rise to a larger error term $\varepsilon$ and thus more influence with regard to evaluating the parameter $m_l$. The approach we employ allows for multiple forgetting factors, which is described in more detail in Ref. [25] and references therein. The following assignments are made:

$$\begin{aligned}
&y(t) = V(t) \\
&x_1 = I_c \qquad && m_1 = R + R_{ct_c} \\
&x_2 = I_d \qquad && m_2 = R + R_{ct_d} \\
&x_3 = \left(\frac{dI}{dt}\right)_c \qquad && m_3 = RR_{ct_c}C_c \\
&x_4 = \left(\frac{dI}{dt}\right)_d \qquad && m_4 = RR_{ct_d}C_d \\
&x_5 = \left(\frac{dI}{dt}\right)_c \qquad && m_5 = R_{ct_c}C_c \\
&x_6 = \left(\frac{dI}{dt}\right)_d \qquad && m_6 = R_{ct_d}C_d \\
&x_7 = 1 \qquad && m_7 = V_{oc}
\end{aligned} \tag{6}$$

The seven $m_l$ parameters are updated at each time step, based on which model parameters are being regressed. Using the regressed model parameters, we deduce the SOC and SOP with methods used previously [29] and summarized as follows:

$$\mathrm{SOC} = w(\mathrm{SOC}_C) + (1 - w)(\mathrm{SOC}_V) \tag{7}$$

In this equation, $w$ is a weighting parameter that is set as an input, $\mathrm{SOC}_c$ is the state of charge as calculated by charge integration, and $\mathrm{SOC}_v$ is related to $V_{oc}$ by means of the $V_{oc}$ vs. SOC curve depicted in Fig. 2. A curve-fit to the average of the charge and discharge curves was employed for the look-up table for the $\mathrm{SOC}_v$ estimation in the DD algorithm. $\mathrm{SOC}_c$ is calculated real-time in recursive fashion:

$$\mathrm{SOC}_c(t) = \mathrm{SOC}(t - \Delta t) + \frac{100 I(t) \Delta t}{Ah_{\mathrm{nominal}}} \tag{8}$$

In the above equation, the nominal capacity $A_h$ is the Ampere-hours of capacity the battery delivers when discharged from 100% to 0% SOC at low rates. The factor 100 is employed to keep a consistent percent basis. We ignore the self-discharge and current inefficiencies.

The SOP is calculated by estimating the charge and discharge power capabilities in real-time. The charging power capability is obtained when the battery voltage is set to its maximum value, and the discharging power capability is obtained when the voltage is set to its minimum. For example:

$$P_{\mathrm{charge(discharge)}}(t) = I_{\mathrm{charge(discharge)}}(t) V_{\mathrm{max(min)}} \tag{9}$$

With the updated parameters and the current $I$ and voltage $V$, we can deduce $I(t)$ once the constant voltage is set at its maximum or minimum value. For the charge current:

$$I_{\mathrm{charge}}(t) = \frac{V_{\max} - V_{oc}}{R + R_{ct\_c}} + \left( \frac{V_{\max} - V + IR}{R} - \frac{V_{\max} - V_{oc}}{R + R_{ct\_c}} \right) \exp\left( -\frac{R + R_{ct\_c}}{RR_{ct\_c}C_c} t \right) \tag{10}$$

and for the discharge current:

$$I_{\mathrm{discharge}}(t) = \frac{V_{\min} - V_{oc}}{R + R_{ct\_d}} + \left( \frac{V_{\min} - V + IR}{R} - \frac{V_{\min} - V_{oc}}{R + R_{ct\_d}} \right) \exp\left( -\frac{R + R_{ct\_d}}{RR_{ct\_d}C_d} t \right) \tag{11}$$

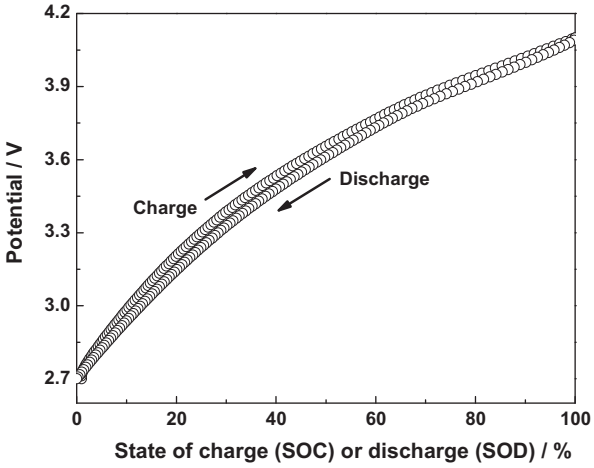


**Fig. 2.** The measured data of the cell potential of the lithium ion battery as a function of SOC. The SOC was deduced by coulomb counting. The measurements were conducted at C/3 rate and at room temperature.

## 3. Testing the DD algorithm with simulated data

The previous section summarizes the DD algorithm including formulas and procedures used for SOC and SOP prediction. In order to examine the regression accuracy of the DD algorithm, software implemented within a test environment was employed along with simulated data. The procedure for the simulation is as follows. First, values are prescribed for model parameters of the RC circuit. Next, based on the values of $I(t)$, voltage data $V(t)$ are determined, and the calculated values for $I(t)$ and $V(t)$ are employed for real-time regression. Finally, the effectiveness of the algorithm is assessed by comparing the regressed parameter values to the prescribed values.

As an example of the simulation tests, the current data was synthesized by adding together four sine waves with random initial phases. The frequencies of the sine waves were 0.001, 0.01, 0.1, and 1 Hz, with an amplitude of 10 A. The time interval of the current data was 100 ms. The selected frequencies and the amplitudes are representative values for traction battery applications. Model parameters were prescribed as:

$$R = 0.0024\,\Omega, \qquad R_{ct\_c} = R_{ct\_d} = 0.0032\,\Omega,$$
$$C_c = C_d = 4500\,\mathrm{F}, \qquad V_{oc} = 3.6\,\mathrm{V}.$$

Using the data stream and the selected parameters, the system voltage was calculated using the circuit model and is shown in Fig. 3. Next, $I$ and $V$ data were input into the algorithm to obtain

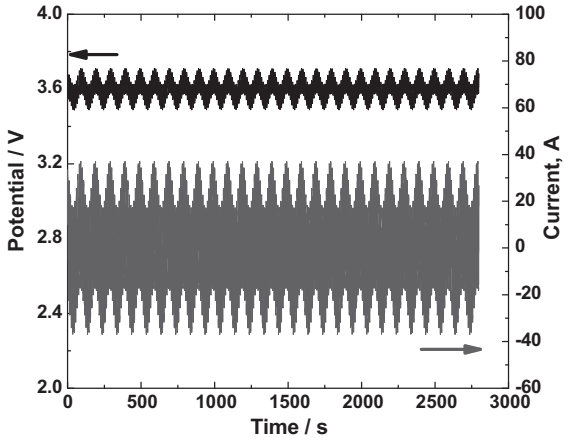


**Fig. 3.** Synthesized current data and deduced voltage data from the ideal circuit model depicted in Fig. 1.

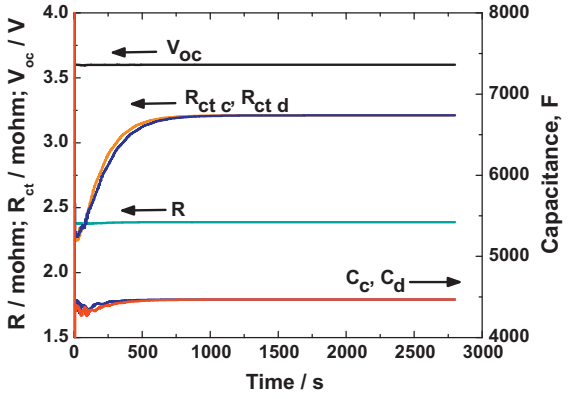


**Fig. 4.** Regression of the model parameters based on the simulated *I–V* data.

the regressed model parameters shown in Fig. 4. The initial values of the parameters were chosen to be

$$R = 0.004\,\Omega, \qquad R_{ct\_c} = R_{ct\_d} = 0.0025\,\Omega, \qquad C_c = C_d = 4000\,\mathrm{F}$$

and the initial $V_{oc}$ was set equal to the first value of the voltage data. The forgetting factors were set to 0.999 for every parameter. As seen in Fig. 4, the regressed values of the parameters are almost identical to the selected values, demonstrating the algorithm's accuracy in parameter regression. We also found that the regression was effectively insensitive to the initial values.

## 4. Experimental setup

In order to evaluate the algorithm in predicting real-time battery states under simulated driving conditions, the algorithm was implemented and integrated with the battery testing system, or a Hardware-in-the-Loop (HWIL) system. [31] The architecture of the HWIL consists of three components: the electrochemical cell (EC) interface, the vehicle model, and the HWIL controller. The EC acts as an environmental interface to the electrochemical cell under test, and its main facilities include a single-channel tester (BT2000, Arbin Instruments) that provides up to 5 kW at potentials between 0.6 and 5 V ± 1 mV and current ranges up to 1 kA ± 10 mA, and a thermal control chamber for accommodating the battery with a programmable range from −40 to 130 °C (resolution of ±10 °C). All tests were conducted at room temperature. The vehicle model used was the Hybrid Powertrain Simulation Program (HPSP) provided by GM. HPSP was applied to provide electric-power requirements

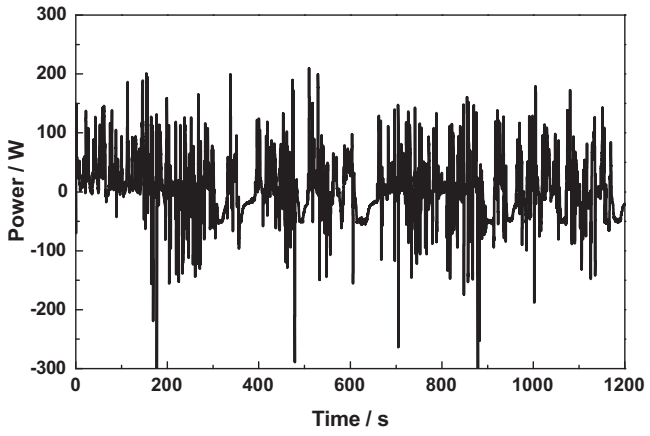


**Fig. 5.** The Milford city driving (power) profile used by HPSP vehicle model to generate the power requirement from the battery.

based on specific driving profiles. The HWIL controller also served as the command center in safeguarding the process. For example, in a cycling process, as a power request is received from HPSP, the HWIL controller analyzes the request and, if valid, sends the request to the EC interface, receives the *I–V–T* response from the interface, iterates through the algorithm with the *I–V–T* data, and provides feedback to the HPSP for its preparation of its next power request. Concurrently, the HWIL controller must continuously monitor the system to ensure operation within specified limits so as to avoid cell abuse. The communications between the above mentioned modules are realized with TCP/IP protocols. The temporal jitter of the recorded data is about a few milliseconds.

The battery used in the experiments was a single-cell lithium ion battery (Hitachi Automotive Products, model #A23-06H04-G00), which has a nominal capacity of 5.6 Ah and a voltage range of 2.7–4.1 V. A driving profile as shown Fig. 5, termed the Milford city profile, was used by HPSP to submit the power demand to the cell. The algorithm was tested by comparing predicted and measured SOC and SOP values with the following procedures.

An initial SOC value was randomly selected (ranging between 30% and 70%), and the corresponding open circuit potential $V_{oc}$ obtained via the look-up table of the voltage-based state of charge. The battery was charged or discharged with a current rate of C/6 until reaching the value of $V_{oc}$, where it was allowed to rest for 20 min (to render an accurate estimation of the initial $V_{oc}$).

The cycling process was initiated (after at least 10 min of cycling). The battery voltage and current was updated every 125 ± 5 ms.

**Table 1**
Initial (seed) values and bounds for the parameters used for the regression of the DD algorithm.

| Quantity (units) | Initial value | Boundary values [min, max] |
|---|---|---|
| $R$ (mΩ) | 4 | [0.4, 40] |
| $R_{ct,c}$ (mΩ) | 2.5 | [0.25, 25] |
| $R_{ct,d}$ (mΩ) | 2.5 | [0.25, 25] |
| $C_c$ (F) | 4000 | [400, 40,000] |
| $C_d$ (F) | 4000 | [400, 40,000] |
| $V_{oc}$ (V) | Measured voltage – value at $t = 0$ | [2.7, 4.1] |
| $w$ (weighting factor) | 0.995 | |
| $A_h$ nominal (Ah) | 5.6 | |
| $V_{min}$ (SOC) (V) | 2.7 | |
| $V_{min}$ (power) (V) | 2.9 | |
| $V_{max}$ (power) (V) | 4.0 | |

The forgetting factor for each parameter was set to 0.999 in this work.

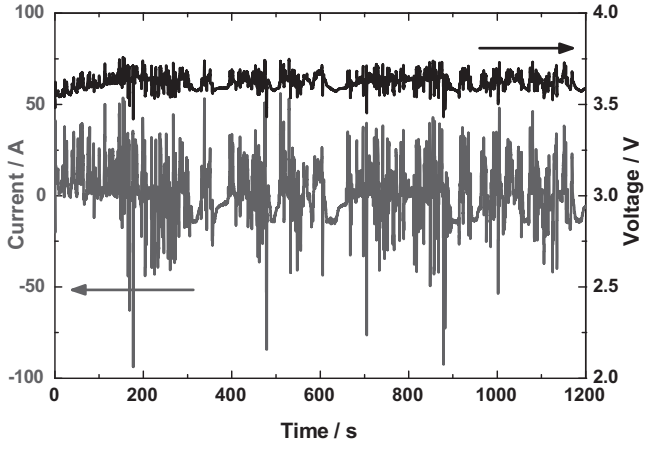


**Fig. 6.** The measured battery current and voltage by the electrochemical cell (EC) interface during the cycling process.

The cycling process was stopped at a random time determined during the initial cycling process, and a choice of test (either SOC test, max charge power test, or max discharge power test) was randomly selected.

In the case of the SOC test, the battery was rested for 1 h at the randomly selected time, and then discharged with a constant current rate of C/3 until battery voltage dropped to its minimum value of 2.7 V. The SOC was deduced by multiplying the discharge current with the discharge time divided by the battery's capacity.

The charge or discharge power tests were performed by commanding the maximum or minimum voltage, respectively, on the battery and tracing its current as a function of time. The charge or discharge power capability as a function of time was determined by multiplying the current-time projection with the maximum or minimum voltage, respectively.

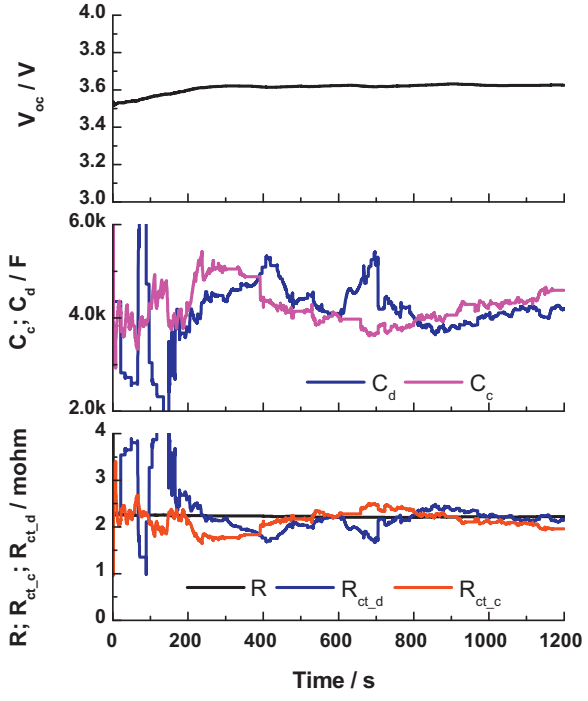


**Fig. 7.** The regressed parameters as the function of time during the cycling process for a random test.

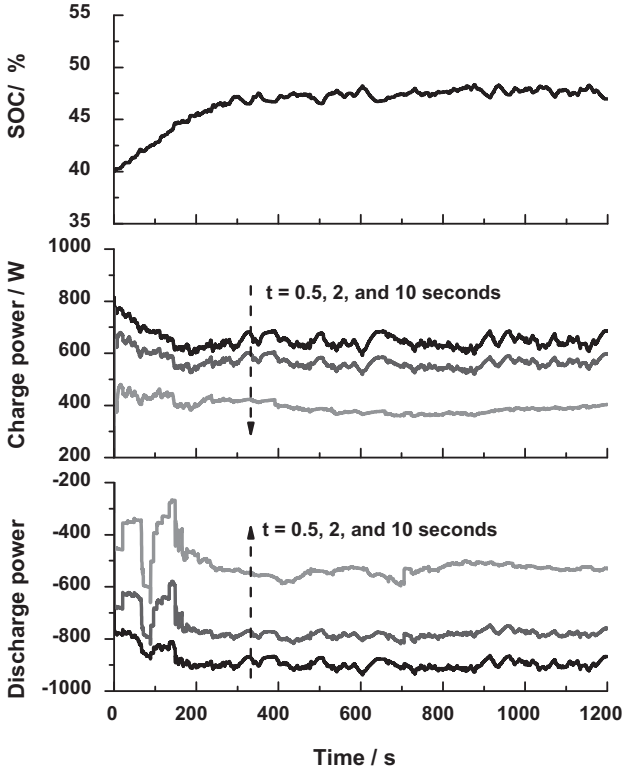


**Fig. 8.** The predicted SOC, charge and discharge power projections at $t = 0.5$, 2, and 10 s during the cycling process.

## 5. Experimental results and discussions

Initial execution of the DD algorithm for regressing the model parameters in real-time requires setting values for certain parameters and their allowed bounds. This is necessary since in a real vehicle environment, noise due to electro-magnetic interference (EMI) may lead the regression to spurious predictions. The initial value and allowable value (boundaries) of each parameter used in the experiments are tabulated in Table 1. As shown in the table, the upper and lower boundaries for the parameter values are set to be ten times larger or smaller than the initial values. In the present work, all $\lambda$s were set to 0.999 for simplicity. The initial value of the parameter $V_{oc}$ was set to be the measured $\Delta t = dt/1 - \lambda = 125$ s voltage at the start of the regression. The sampling period $dt$ was 125 ms, thus was approximately the time-duration over which past data impact the regression (cf. Eq. (12) in Ref. [29] and discussions therein). It should be noted; however, the algorithm keeps the capability in fine-tuning each $\lambda$ to improve the regression accuracy. For instance, the value of $\lambda$ for $V_{oc}$ would be set smaller to capture fast SOC variations with current.

As an example of a random trial, a test of charge power capability is highlighted in detail before discussing the final random test results. Fig. 6 depicts the measured current and voltage of the battery during the cycling process. Based on initial values, boundary conditions, forgetting factors of the parameters and the updated variables $I$, $V$ of the battery, the DD algorithm regressed the model parameters recursively with their final values depicted in Fig. 7. As shown in the figure, the high-frequency resistance $R$ remains almost the same throughout the driving process, consistent with a constant number of charge carriers in the electrolyte phases, and little change in the solid phase electronic resistance in the lithium ion battery. The open-circuit potential $V_{oc}$ increases slightly due to the fact that the driving profile has more charge cases than discharge cases. There are quantitative differences between

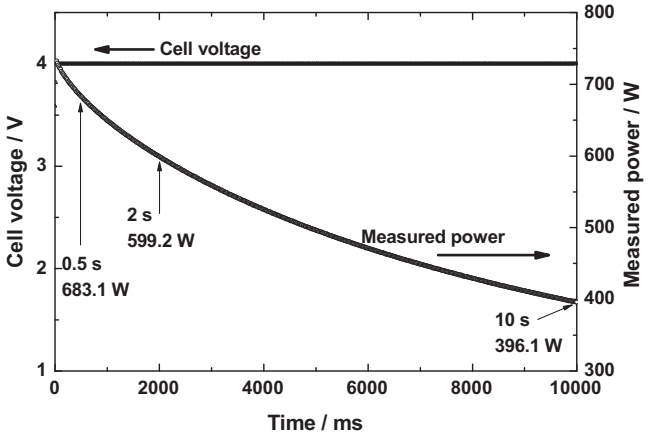


**Fig. 9.** The measured discharging power of the battery verse time as the battery voltage is clamped at 4 V after the 1200s of excitation depicted in Fig. 8.

**Table 2**
The comparison between the predicted powers with the measured powers at three different projected times after the 1200s of excitation depicted in Fig. 8 (cf. Fig. 9).

| Projected time | Predicted power | Measured power | Difference |
|---|---|---|---|
| 0.5 s | 687.1 W | 683.1 W | 0.5% |
| 2 s | 599.4 W | 599.2 W | 0.03% |
| 10 s | 405.8 W | 396.1 W | 2.5% |

the regressed charge and discharge parameter values for charge-transfer resistance and capacitance. All parameters were regressed within their preset boundary values, indicative of algorithm stability. The discharge parameters have some cusps at the beginning of the cycling process because there was not enough discharge information to enable a stable regression. With the updated parameters, the algorithm predicted SOC and SOP real-time with the results shown in Fig. 8. The SOC increases in the beginning period of 200 s and then remains nearly constant, consistent with the driving profile. As mentioned earlier, the DD algorithm uses Eqs. (9)–(11) to predict power capabilities. Fig. 8 demonstrates the predicted SOCs as well as charge and discharge power projections at $t = 0.5, 2, 10$ s during the cycling process. At the end of the cycling, as the cycling duration reached 1200s in this example, the charge power test

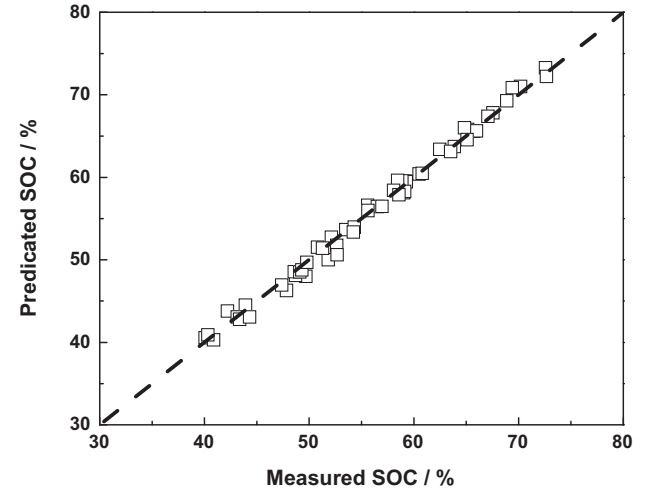


**Fig. 10.** Summary of random SOC tests. Each square corresponds to a randomly selected point within the cycle to perform the SOC test, with the measured value provided by the abscissa; the algorithm-predicted SOC for the test is provided on the ordinate.

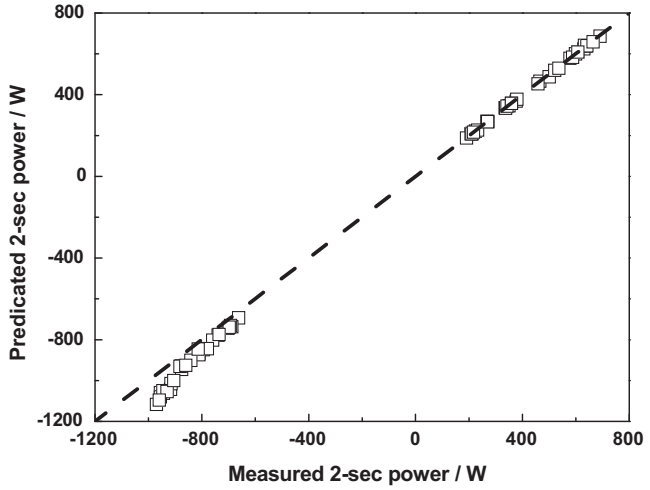


**Fig. 11.** Summary of random tests for the 2 s SOP tests. Each square corresponds to one of the random tests; algorithm-predicted 2 s power projections correspond to the ordinate, and the abscissa values reflect measurements.

was performed on the battery with results presented in Fig. 9. In the measurement, the battery voltage was clamped to 4 V, corresponding to the maximum voltage $V_{max}$ used in the algorithm for calculating the power capabilities. The battery's current, and consequently the power, were then sampled with 0.1 s interval and recorded for 10 s. Predicted values of the charge power were compared with the measured values, and the results are presented in Table 2. The measured values agree with the predicted values for the 0.5 s and 2 s power results, while the 10 s power projections show a larger deviation. In general, SOP prediction accuracy is greater for shorter time intervals; the short-term power is mainly determined by the high-frequency resistance $R$, and the regression of $R$ is stable and accurate, leading to accurate short-term power predictions.

Figs. 10–12 summarize the results of 150 random tests on SOC and SOP. Each data point in the figures corresponds to a random test. In Fig. 10, the predicted values of SOC are within ±3% accuracy relative to the measured values. The errors are likely due to numerical errors in coulomb integration. Since the weighting factor $w$ was initialized with 0.995 in the algorithm, the agreement of SOC results verifies that for this battery, the SOC is dominated

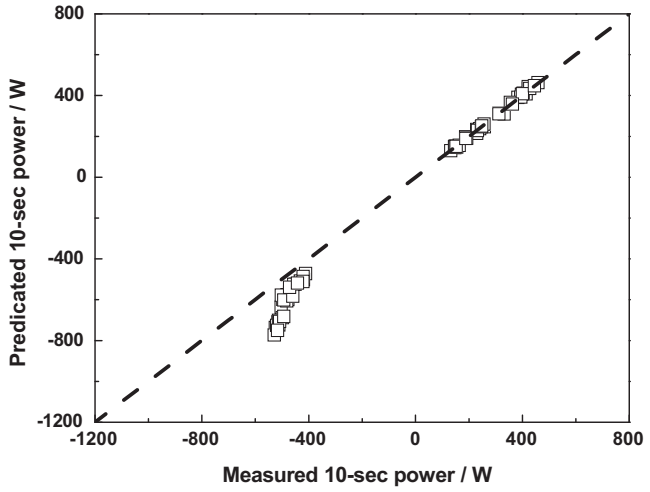


**Fig. 12.** Summary of random tests for the 10 s SOP tests. Each square corresponds to one of the random tests; algorithm-predicted 10 s power projections correspond to the ordinate, and the abscissa values reflect measurements.

by coulomb counting. Fig. 11 demonstrates the predicted 2 s power projections against the measured values. The positive values correspond to charge power tests, while the negative values refer to discharge power tests. The charge power projections are quite accurate, while the discharge power projections are larger than those measured. The deviations tend to grow as the power magnitude increases. Fig. 12 compares the predicted 10 s power projections with measured values. Similar to the 2 s results, predictions of the charge power capabilities are excellent, while the predicted discharge powers are larger than those measured, and the deviation becomes larger as the power magnitude increases.

## 6. Summary and open questions

A multi-parameter battery state estimator has been developed and tested on lithium ion batteries in a vehicle environment. The algorithm is based on the adaptive and direct solution of the governing differential equations that characterize the equivalent circuit representation of the battery. We refer to the approach as a direct differential algorithm. The results appear to be quite promising. The algorithm predicts the lithium ion battery SOC quantitatively. The 2 s power prediction is excellent on charge and good on discharge. The 10 s power prediction is again quite good on charge; however, further improvement is desirable for discharge power projection.

The DD algorithm appears to represent a significant improvement over our existing superposition integral algorithm. The DD regression is much more stable over representative cycling processes and did not exhibit severe sensitivity to initial (seed) values. We believe the DD algorithm will find broader application in battery-control systems. It should be noted that all the experiments are conducted in the lab environment and sensor noises are not critical. In a real vehicle environment with substantial signal noises, a Kalman filter may need to be included to optimize the regression.

There are several open issues relative to improving the algorithm.

*The SOH issue*. How to estimate SOH in the DD algorithm was neglected. SOH is related to battery aging and is much more difficult to predict than SOC and SOP. The aging mechanisms are complicated and may be different for each type of lithium ion battery. In Ref. [10], the SOH was defined as $\mathrm{SOH} \equiv R_{\mathrm{nominal}}(T, \mathrm{SOC})/R(T, \mathrm{SOC})$. This definition captures the mechanism that the aging is mainly due to the electrode degradation with time, commensurate with the increase of the high-frequency resistance. However, for some lithium ion batteries, aging is mainly due to the decrease of active lithium ions within the battery (capacity loss) and the high-frequency $R$ does not change much. In this case, the aging symptom mainly manifests in the decrease of the battery capacity Ah. We are investigating the possibility of monitoring the Ah change, and therefore SOH, with the DD algorithm.

*Forgetting factors* $\lambda$. As mentioned in previous sections, varying the values of $\lambda$ can influence the regression of the DD algorithm. However, the optimization of the values of $\lambda$ is strongly dependent on the sampling rate as well as driving profile. It may be much more meaningful to dynamically adjust the values of $\lambda$ based on the skewness of the driving profile, and this should be investigated.

*10 s power deviation*. As the power tests have shown, the 10 s discharge power projections are larger in magnitude than measured values and the deviation is more severe as the magnitude increases. We have found that this is not due to the algorithmic approach; rather, it is due to the limitation of the single-RC-circuit model. For the batteries we have tested, diffusion phenomena become important in the discharging case beyond a few seconds.

## Acknowledgements

We appreciate the help of Souren Soukiezian of HRL in setting up the experiments and measuring the initial battery capacities, Andy Nowak of HRL in editing and comments, and Brian Koch of GM Product Development in providing the Milford-city driving profile.

## References

[1] M. Armandand, J.M. Tarascon, Nature 451 (2008) 652.
[2] J.M. Tarascon, M. Armand, Nature 414 (2001) 359.
[3] A.S. Arico, P. Bruce, B. Scrosati, J.M. Tarascon, W. Van Schalkwijk, Nat. Mater. 4 (2005) 366.
[4] M.S. Whittingham, Chem. Rev. 104 (2004) 4271.
[5] I. Bloom, B.W. Cole, J.J. Sohn, S.A. Jones, E.G. Polzin, V.S. Battaglia, G.L. Henriksen, C. Motloch, R. Richardson, T. Unkelhaeuser, D. Ingersoll, H.L. Case, J. Power Sources 101 (2001) 238.
[6] M. Broussely, S. Herreyre, P. Biensan, P. Kasztejna, K. Nechev, R.J. Staniewicz, J. Power Sources 97–8 (2001) 13.
[7] B. Kang, G. Ceder, Nature 458 (2009) 190.
[8] M. Verbrugge, in: M. Schelsinger (Ed.), Modern Aspects of Electrochemistry: Modeling and Numerical Simulations I, vol. 43, 1st ed., Springer, 2009 (Chapter 8).
[9] M. Doyle, T.F. Fuller, J. Newman, J. Electrochem. Soc. 140 (1993) 1526.
[10] J. Newman, W. Tiedemann, AIChE J. 21 (1975) 25.
[11] A.P. Schmidt, M. Bitzer, Á.W. Imre, L. Guzzella, J. Power Sources 195 (2010) 5071.
[12] K.A. Smith, Control Syst. Mag. IEEE 30 (2010) 18.
[13] N.A. Chaturvedi, R. Klein, J. Christensen, J. Ahmed, A. Kojic, Control Syst. Mag. IEEE 30 (2010) 49.
[14] Y. Hu, S. Yurkovich, Y. Guezennec, R. Bornatico, American Control Conference 2008, 2008, p. 318.
[15] P.L. Moss, G. Au, E.J. Plichta, J.P. Zheng, J. Electrochem. Soc. 155 (2008) A986.
[16] P. Pisu, G. Rizzoni, Vehicle Power and Propulsion, 2005 IEEE Conference, 2005, p. 8.
[17] G.L. Plett, J. Power Sources 134 (2004) 252.
[18] S. Santhanagopalan, Q.Z. Guo, P. Ramadass, R.E. White, J. Power Sources 156 (2006) 620.
[19] S. Santhanagopalan, R.E. White, J. Power Sources 161 (2006) 1346.
[20] S. Santhanagopalan, R.E. White, Int. J. Energy Res. 34 (2010) 152.
[21] Y. He, W. Liu, B.J. Koch, J. Power Sources 195 (2010) 2969.
[22] H. Asai, H. Ashizawa, D. Yumoto, H. Nakamura, Y. Ochi, SAE Trans. 114 (2005) 205.
[23] W. van Schalkwijk, B. Scrosati, Adv. Lithium-Ion Batteries (2002).
[24] L. Cai, R.E. White, J. Power Sources 196 (2011) 5985.
[25] M. Verbrugge, J. Appl. Electrochem. 37 (2007) 605.
[26] M. Verbrugge, E. Tate, J. Power Sources 126 (2004) 236.
[27] S. Pillar, M. Perrin, A. Jossen, J. Power Sources 96 (2001) 113.
[28] M. Verbrugge, D. Frisch, B. Koch, J. Electrochem. Soc. 152 (2005) A333.
[29] M. Verbrugge, B. Koch, J. Electrochem. Soc. 153 (2006) A187.
[30] M.W. Verbrugge, R.S. Conell, J. Electrochem. Soc. 150 (2003) A1153.
[31] C. Massey, A. Bekaryan, M. Verbrugge, T. Weber, D. Frisch, L. Turner, A. Perulian, P. Liu, SAE Commercial Vehicle Engineering Conference, SAE International, Warrendale, PA, 2005.
[32] M.W. Verbrugge, R.S. Conell, J. Electrochem. Soc. 149 (2002) A45.
[33] M.W. Verbrugge, R.Y. Ying, J. Electrochem. Soc. 154 (2007) A949.
[34] A. Vahidi, A. Stefanopoulou, H. Peng, Vehicle Syst. Dyn. 43 (2005) 31.